

Optically induced magnetization dynamics and variation of damping parameter in epitaxial Co_2MnSi Heusler alloy films

Y. Liu, L. R. Shelford, V. V. Kruglyak, and R. J. Hicken

School of Physics, University of Exeter, Stocker Road, Exeter, EX4 4QL, United Kingdom

Y. Sakuraba, M. Oogane, and Y. Ando

Department of Applied Physics, Graduate School of Engineering, Tohoku University, Sendai 980-8579, Japan

(Received 17 June 2009; revised manuscript received 7 January 2010; published 1 March 2010)

All-optical pump-probe measurements of magnetization dynamics have been performed upon epitaxial $\text{Co}_2\text{MnSi}(001)$ Heusler alloy thin films annealed at temperatures of 300, 400, and 450 °C. An ultrafast laser-induced modification of the magnetocrystalline anisotropy triggers precession which is detected by time-resolved magneto-optical Kerr effect measurements. From the damped oscillatory Kerr rotation, the frequency and relaxation rate of the precession is determined. Using a macrospin solution of the Landau-Lifshitz-Gilbert equation the effective fields acting upon the sample magnetization are deduced. This reveals that the magnetization is virtually independent of the annealing temperature while the fourfold magnetocrystalline anisotropy decreases dramatically with increasing annealing temperature as the film structure changes between the B2 and $L2_1$ phases. From the measured relaxation rates, the value of the apparent Gilbert damping parameter is found to depend strongly upon the static field strength and in-plane static field orientation. The variation of the apparent damping parameter is generally well reproduced by an inhomogeneous broadening model in which the presence of B2 and $L2_1$ phases leads to a large dispersion of the magnetocrystalline anisotropy. However, for the sample annealed at a temperature of 300 °C, the lack of a detailed fit to the data suggests that the apparent anisotropy of the apparent damping parameter might alternatively arise due to a network of dislocations with fourfold symmetry.

DOI: [10.1103/PhysRevB.81.094402](https://doi.org/10.1103/PhysRevB.81.094402)

PACS number(s): 75.40.Gb, 76.50.+g, 75.30.-m, 75.30.Gw

I. INTRODUCTION

Heusler alloys have recently attracted great interest for use in spintronic devices since high spin polarization and even half-metallic behavior can be realized in some phases.¹ Recently, it has been shown that epitaxial films may be obtained by sputter deposition and postdeposition annealing,² and large room temperature tunnel magneto-resistance (TMR) values have been observed in magnetic tunnel junctions (MTJs) in which Co_2MnSi Heusler alloys were used as electrodes.³ Furthermore, it is expected that the half-metallic band structure may suppress spin-flip processes, leading to reduced magnetic damping and hence lower critical currents in spin transfer torque devices. Recently, a damping parameter of 0.0023 was reported for a NiMnSb film measured by resonant cavity ferromagnetic resonance.⁴ The full exploitation of Heusler alloys requires an improved understanding of the intricate relationship between structural and magnetic properties, and particularly dynamic magnetic properties such as damping.

While it is possible to manipulate the magnetic properties of Heusler alloys by substitution of different chemical species at different atomic sites, this paper is concerned solely with the Co_2MnSi model system. Epitaxial $\text{Co}_2\text{MnSi}(001)$ films have been obtained by sputter deposition onto single crystals of $\text{MgO}(100)$ with a Cr buffer layer,⁵ with x-ray diffraction being used to identify the crystallographic phase. Films deposited at ambient temperature adopt the A2 phase in which the Co, Mn, and Si ions are randomly located upon a body centered cubic lattice. Post-deposition annealing leads first to the formation of the B2 phase in which the Co

ions order into a simple cubic lattice, with the Mn and Si ions randomly occupying the body center sites. As the annealing temperature is increased the more highly ordered $L2_1$ phase is obtained in which the Mn and Si ions occupy alternate body center sites. The fraction of the $L2_1$ phase within the film can be deduced from a careful analysis of different peak intensities in x-ray diffraction experiments, and was confirmed to increase continuously with annealing temperature, T_{an} .⁶ Magnetometry measurements of bulk $L2_1$ Co_2MnSi yield a low temperature magnetization of 138 emu/g (Ref. 7) corresponding to a value of 1030 emu/cm³ for a lattice parameter of 0.565 nm. Since Co_2MnSi has a Curie temperature of 985 K,⁷ the room temperature magnetization is expected to be close to 1000 emu/cm³. However, recent SQUID magnetometry measurements made upon epitaxial films yielded a reduced magnetization,⁵ its value falling from 850 to 800 emu/cm³ as T_{an} was increased from 350 to 500 °C.⁶ In this case, the magnetization was found to be only weakly dependent on temperature in the range of 2–300 K (Ref. 8) suggesting that the Curie temperature remained high. A fourfold anisotropy with the easy axes corresponding to the $\langle 110 \rangle$ axes of the Co_2MnSi was observed.⁶ The cubic anisotropy constant K_1 had a value of -0.9×10^5 erg/cm³ for $T_{\text{an}}=375$ °C, decreasing in magnitude to $K_1=-0.1 \times 10^5$ erg/cm³ for $T_{\text{an}}=450$ °C. While the dependence of the magnetic properties upon T_{an} might be related to the changing fraction of the $L2_1$ phase present in the films, the authors could not exclude the possibility that annealing promoted diffusion of Cr from the buffer layer into the Co_2MnSi film.

Since the TMR observed in MTJ structures is largely determined by the properties of the electrode-tunnel barrier in-

interface, measurements sensitive to the near interfacial region have recently been performed upon Co_2MnSi films capped with thin layers of plasma oxidized aluminum oxide. X-ray magnetic circular dichroism (XMCD) measurements, performed in total electron yield mode, probe a near interface region of 1 to 2 nm thickness that is determined by the escape length of the secondary electrons. Such measurements were performed upon the series of samples for which dynamic measurements will be presented in the present paper and which have been labeled A_x where x is the annealing temperature in the range of 300–500 °C.⁹ The Co and Mn x-ray absorption spectra revealed both x-ray absorption near edge structure (XANES) and extended x-ray absorption fine structure (EXAFS) oscillations that confirmed that $L2_1$ ordering improved with increasing annealing temperature. Magnetic moments were observed on both the Co and Mn sites, but for these samples the moment per 3d hole was found to be independent of annealing temperature in the range of 300–500 °C at 0.35 μ_B and 0.4 μ_B for Co and Mn, respectively,⁹ the number of 3d holes not being precisely known. The emergence of a multiplet structure in the XMCD spectra was attributed to the localization of minority spins in the half-metallic state. A further study confirmed that the magnetization of the near interface region remained constant within experimental error between liquid Helium and room temperatures.¹⁰ Magnetic second harmonic generation (MSHG) measurements were performed upon this same set of samples in order to probe the magnetic response of the $\text{Co}_2\text{MnSi}/\text{AlO}_x$ interface.¹¹ The MSHG was found to depend upon whether the magnetic field was applied parallel to an easy or hard axis, and this anisotropy in the MSHG was shown to be well correlated with the TMR achieved in MTJs fabricated with similar electrodes.

Yilgin *et al.* have used X-band ferromagnetic resonance (FMR) to study the dynamic properties of epitaxial Co_2MnSi thin films.¹² The samples were rotated so that the orientation of the magnetic field varied either within the plane of the film, or from an in-plane to an out of plane configuration. The magnetization and the magnitude of K_1 were observed to decrease dramatically as T_{an} increased from 300–500 °C. The variation of the FMR linewidth was fitted by a model¹³ that allowed the inhomogeneous broadening contribution to the total linewidth to be removed.¹⁴ However, for the film annealed at 300 °C the damping parameter extracted after removal of the inhomogeneous broadening contribution was found to be anisotropic, with a value of 0.003 when the field was parallel to the easy axis, and 0.006 when the field was parallel to the hard axis. This damping parameter was found to increase with increasing annealing temperature, while the anisotropy of the damping parameter was reduced at higher annealing temperatures.

Recent studies have shown that the damping of precessional dynamics in ferromagnetic metals can be complicated by the action of many extrinsic damping processes such as inhomogeneous broadening,¹⁵ two-magnon scattering,^{16–18} interface effects,¹⁹ and spin diffusion into adjacent metallic layers,^{14,15,20} with Cr in particular shown to be a strong spin scatterer.²¹ Müller *et al.* observed a sharp increase in the damping in CrO_2 films above a threshold pump fluence, possibly due to spin-wave instabilities.²² Differences in damping

have been found when direct comparison has been made between different frequency, field and time domain techniques.²³ Time-resolved optical measurements have the advantage that they can probe a much smaller volume than microwave resonance experiments, but may be susceptible to additional contributions to the damping. For example, the spatial profile of a pulsed magnetic field or a focused pump laser spot may lead to the generation of magnons that propagate away from the region that is being probed. Eilers *et al.*²⁴ performed simulations of nonlocal damping by spin-wave emission and found that spin-wave emission becomes a significant damping mechanism when the excitation area is less than 1 μm , while Wu *et al.*²⁵ showed that propagation of magnetostatic spin waves could be significant even for probed regions of tens of microns in size.

In this paper an all-optical time-resolved magneto-optical Kerr effect (TRMOKE) study of the magnetization dynamics of epitaxial Heusler alloy Co_2MnSi thin films will be presented. Ultrafast heating by laser pulses is used to induce magnetization dynamics through the temperature dependence of the magnetic anisotropy.^{26–30} The technique has the advantage of allowing the magnetization dynamics to be studied over a continuous range of frequencies. By fitting the time dependent Kerr signals to a macrospin solution of the Landau-Lifshitz-Gilbert (LLG) equation, values are obtained for the effective fields acting upon the magnetization and values for the cubic anisotropy constant and total apparent damping parameter are deduced. The presence of different putative extrinsic damping mechanisms will be considered, and the data will be fitted to a generalized model of inhomogeneous broadening.

II. EXPERIMENTAL PROCEDURE

Co_2MnSi thin films of 30 nm thickness were deposited by magnetron sputtering upon $\text{MgO}(001)$ substrates coated with a 40 nm buffer layer of Cr.³¹ The films were annealed at temperatures up to 450 °C to improve the lattice structure and the atomic ordering among Co, Mn, and Si sites. The films were finally capped with 1.3 nm of Al. In this paper, we focus our investigation on three samples: sample A_{300} , annealed at 300 °C has the B2 structure; A_{400} and A_{450} annealed at 400 °C and 450 °C, respectively, have predominantly the $L2_1$ structure. X-ray diffraction analysis confirmed that the films possessed the (001) orientation with the [100] and [110] axes of the film being aligned with the [110] and [010] axes of the MgO substrate.

The static magnetic properties of the Co_2MnSi films were investigated by vibrating sample magnetometry (VSM), and longitudinal magneto-optical Kerr effect (MOKE) magnetometry measurements performed with a 633 nm He-Ne laser with intensity stability of better than 0.1%.³² In MOKE measurements, the sample and electromagnet were mounted on separate rotating mounts so that the magnetic field could be applied at any orientation within the plane of the film, and the longitudinal MOKE could be used to sense the in-plane component of magnetization either parallel or perpendicular to the field.³³ In this way, the hard and easy axes of the samples could be quickly identified at room temperature and the saturation fields determined.

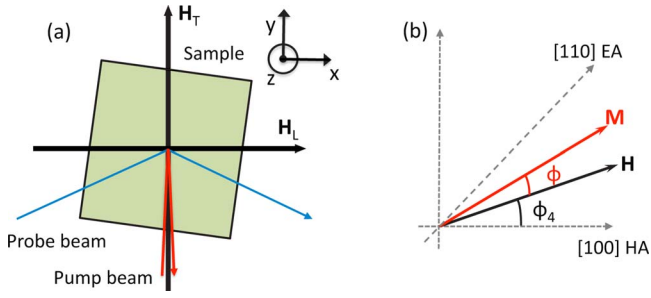


FIG. 1. (Color online) (a) Orientation of sample, applied field, and probe beam. Two orientations of the static field were used. \mathbf{H}_L and \mathbf{H}_T are parallel and perpendicular to the plane of incidence, respectively. (b) Definition of the angles ϕ and ϕ_4 .

Time-resolved optical pump-probe measurements were made using pulses of 100 fs duration from a Ti:sapphire regenerative amplifier. The sample was pumped with the p -polarized 800 nm wavelength output of the amplifier at near normal incidence with pulse energy up to 0.9 μJ . The dynamic magnetization was determined from the Kerr rotation of a time-delayed frequency-doubled 400 nm wavelength s -polarized probe beam. The probe, incident at 40° to the sample normal, had a much weaker pulse energy of 4 nJ, and was focused to overlap with the pump spot on the sample surface. The sizes of the pump and probe spots were typically 140 and 80 μm , respectively. The focusing lenses were mounted on three-axis translation stages so that the overlap of the spots could be adjusted as they were viewed with a high-magnification CCD camera. The pump beam was modulated by a mechanical chopper and phase-sensitive detection was used to detect the dynamic Kerr rotation. Static hysteresis loops were acquired with the probe beam in the absence of the pump in order to calibrate the size of the magneto-optical response.

Assuming that the magnetization lies close to the direction of the applied field prior to the arrival of the pump pulse, the total MOKE signal will generally contain an oscillatory component due to magnetization precession and a component due to ultrafast demagnetization. The demagnetization signal appears as a sharp peak with a rise time of a few hundred fs followed by a decay with ns relaxation time. When the oscillatory signal is small it can be overwhelmed by the demagnetization signal, and in such cases sensitivity to the demagnetization signal can be removed by changing the orientation of the applied static field. Figure 1(a) shows the relative orientation of the sample (xy plane), applied static field and plane of incidence of the probe (xz plane). An s -polarized probe is sensitive to changes of the x and z components of the magnetization due to the longitudinal and polar magneto-optical Kerr effects, respectively. When the static field is applied perpendicular to the plane of incidence (\mathbf{H}_T), the equilibrium magnetization vector is aligned with the y axis, and changes in its magnitude are no longer detected by either the longitudinal or polar Kerr effects, allowing the precessional signal to be more clearly seen.

III. THEORY

The intense optical pump pulse is expected to induce a partial demagnetization of a metallic ferromagnetic sample

on subpicosecond time scales.³⁴ The temperature dependence of the cubic magnetocrystalline anisotropy constant K_1 can be deduced from its dependence upon the magnetization M_S .³⁵ Assuming that increased temperature only introduces local fluctuations of \mathbf{M} and does not affect its local magnitude, and that the total deviation of \mathbf{M} is the result of a large number of small deviations, the temperature variation of the first order anisotropy constant is predicted to have the form $K_1(T) \sim M_S(T)^n$ where n is equal to 10.³⁶ It is therefore reasonable to assume that the demagnetizing and magnetocrystalline anisotropy fields of the sample will be modified on time scales short compared to the period of precession. After pumping, the effective magnetic field will no longer be parallel to the magnetization (unless \mathbf{H} is parallel to the easy or hard axis), and precession will be induced by a torque acting on the magnetization. The oscillatory part of the measured Kerr rotation may be written in the general form,

$$\theta_K \propto \Delta\phi \cos[2\pi(f_0 + bt)t + \varphi] \exp(-t/\tau), \quad (1)$$

where $\Delta\phi$, f_0 , $1/\tau$, and φ are, respectively, the initial amplitude of precession, which is the initial angle of misalignment of the magnetization from equilibrium, the frequency, the relaxation rate, and the initial phase of the precessional signal. The parameter b is included to allow for a chirp that occurs as the values of magnetic parameters such as M_S and K_1 change gradually as the probed volume cools. However, if the chirp is neglected and the values of the magnetic parameters are assumed to be constant after initial modification by the pump, then algebraic expressions may be obtained that relate the frequency, amplitude and relaxation time to the magnetic parameters. The precessing magnetization may be described by the Landau-Lifshitz-Gilbert equation,

$$\frac{\partial \mathbf{M}}{\partial t} = -|\gamma| \mathbf{M} \times \mathbf{H}_{\text{eff}} + \frac{\alpha}{M} \left(\mathbf{M} \times \frac{\partial \mathbf{M}}{\partial t} \right), \quad (2)$$

where α is the phenomenological damping parameter, $\gamma = 2.8 \times \pi \times g$ MHz/Oe is the gyromagnetic ratio of the electron, and $|g|$ is the spectroscopic splitting factor. \mathbf{H}_{eff} is the total effective magnetic field acting upon the magnetization, with contributions from the external magnetic field, the demagnetizing field and the magnetocrystalline anisotropy.

In the limit that $\alpha \ll 1$ the amplitude, frequency and relaxation time can be expressed in terms of the magnetic parameters of the film,²⁹

$$\Delta\phi = \frac{-(1/2)\sin[4(\phi - \phi_4)]\Delta(K_1/M_S)}{H \cos \phi + (2K_1^{(0)}/M_S)\cos[4(\phi - \phi_4)]}, \quad (3)$$

$$f_0 = \frac{1}{2\pi} |\gamma| (H_\alpha H_\beta)^{1/2}, \quad (4)$$

$$\tau = \frac{2}{|\gamma| (H_\alpha + H_\beta) \alpha}, \quad (5)$$

where $\Delta\phi$ is the amplitude of precession and $K_1^{(0)}$ is the room temperature value of the cubic magnetocrystalline anisotropy constant. $\Delta(K_1/M_S)$ is the pump-induced reduction in the anisotropy field at the increased temperature. The effective fields H_α and H_β include contributions from the external

magnetic field, the magnetocrystalline anisotropy and the demagnetizing field (see Ref. 29). At equilibrium the magnetization will align with the effective field. The equilibrium condition is defined as,

$$M_S H \sin \phi + \frac{K_1}{2} \sin[4(\phi - \phi_4)] = 0, \quad (6)$$

where ϕ_4 is the angle between the applied magnetic field and the Co_2MnSi [100] axis, and ϕ is the equilibrium

canting angle between the applied magnetic field and the magnetization. If H is sufficiently large that ϕ is small then Eq. (6) may be expanded to give an explicit algebraic expression for ϕ . At low field, the small angle approximation for the canting angle ϕ becomes invalid, but by retaining quadratic terms in ϕ , the expansions of $\sin \phi$ and $\cos \phi$ are accurate to 2.5% and 1%, respectively. In this case, the value of ϕ is obtained to a reasonable approximation from the expression,

$$\phi = \frac{-[M_S H + 2K_1 \cos(4\phi_4)] + \sqrt{[M_S H + 2K_1 \cos(4\phi_4)]^2 + 8K_1^2 \sin^2(4\phi_4)}}{8K_1 \sin(4\phi_4)}. \quad (7)$$

From the TRMOKE measurements, the value of an apparent damping parameter can be deduced that contains contributions from all the damping processes that are present. Inhomogeneous broadening may occur due to the dephasing of an ensemble of magnetic moments precessing independently with slightly different frequency. Assuming a Lorentzian frequency distribution of form,

$$A(\omega) = \frac{A_0}{(\omega - \omega_0)^2 + (\Delta\omega_{\text{FWHM}}/2)^2}, \quad (8)$$

it may be shown using elementary Fourier analysis that the time dependent Kerr rotation has the form of Eq. (1) but with a modified relaxation rate $1/\tau'$ where $1/\tau' = 1/\tau + 1/\tau_{\text{inhom}}$. The relaxation rate due to inhomogeneous broadening is given by $1/\tau_{\text{inhom}} = \Delta\omega_{\text{FWHM}}/2$, while contributions of other mechanisms to the observed relaxation rate can be included by adding further relevant relaxation rates. In the present case, $1/\tau$ accounts for all other damping mechanisms, including intrinsic damping. The measured apparent damping parameter is derived from Eq. (5) using the modified relaxation rate $1/\tau'$ as follows:

$$\alpha = \frac{2}{|\gamma|(H_\alpha + H_\beta)\tau'} = \frac{2}{|\gamma|(H_\alpha + H_\beta)} \left(\frac{1}{\tau} + \frac{\Delta\omega_{\text{FWHM}}}{2} \right). \quad (9)$$

The contribution to the damping from inhomogeneous broadening is given by,

$$\alpha_{\text{inhom}} = \frac{1}{|\gamma|(H_\alpha + H_\beta)} \left(\left| \frac{\partial\omega}{\partial M_S} \Delta M_S + \frac{\partial\omega}{\partial K_1} \Delta K_1 \right| + \left| \frac{\partial\omega}{\partial \phi_4} \Delta \phi_4 \right| + \left| \frac{\partial\omega}{\partial K_{u\perp}} \Delta K_{u\perp} \right| \right), \quad (10)$$

with ΔM_S , ΔK_1 , $\Delta \phi_4$, and $\Delta K_{u\perp}$ describing the inhomogeneity of the magnetic parameters. The partial derivatives are calculated from Eqs. (4) and (7). A combined contribution of ΔM_S and ΔK_1 is assumed since $K_1(T)$ is known to depend strongly on $M_S(T)$. The significance of damping mechanisms other than intrinsic damping in the value of $1/\tau$ will be tested for by experiment.

IV. EXPERIMENTAL RESULTS

A. Characterization of static magnetic properties

The sample magnetization was measured by VSM and found to have values of 980, 1000, and 1000 emu/cm³ at room temperature for A_{300} , A_{400} , and A_{450} , respectively. The magnetic anisotropy was investigated by means of MOKE magnetometry. Figure 2 shows static hysteresis loops with the field applied parallel to the easy, hard and intermediate axes. The raw data also contained a component quadratic in the sample magnetization,⁶ which was subtracted by symmetry analysis, as demonstrated by Hamrle *et al.*³⁷ No quadratic magneto-optical effect was observed when loops were acquired with a 400 nm wavelength beam, and so Eq. (1) remains applicable in describing the results of TRMOKE measurements.

The loops show a clear fourfold symmetry as the magnetic field is applied in different directions within the plane of the film, with the easy and hard axes lying parallel to the [110] and [100] axes of the Co_2MnSi film, respectively. The magnetocrystalline anisotropy is reduced at higher annealing temperatures, with the hard axis saturation field falling from 260 to 140 Oe then 80 Oe for samples A_{300} , A_{400} and A_{450} , respectively. The easy axis coercive field is about 15 Oe for all three samples. The saturation Kerr rotation at 633 nm wavelength also decreases with increasing annealing temperature, though the VSM measurement showed the magnetization to be virtually unchanged. There is no evidence of any significant in-plane uniaxial anisotropy field.

B. Dependence of transient Kerr rotation signals upon field orientation

Figure 3 shows the ultrafast demagnetization TRMOKE signal obtained within the first few picoseconds after excitation with a 0.6 μJ pump pulse. The transient Kerr rotation signal (left hand column) reaches a maximum within about 650 fs, before decaying to about half the maximum value after the first few ps. Plots of the TRMOKE signal on a logarithmic time scale (not shown) reveal that the decay can

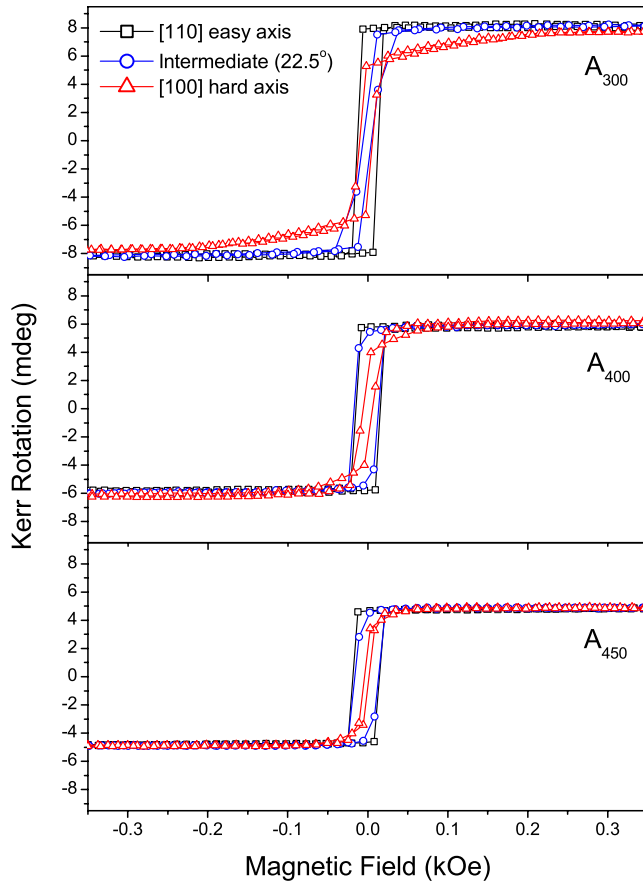


FIG. 2. (Color online) Longitudinal MOKE loops obtained at 633 nm wavelength. All loops are shown after removal of a component quadratic in the magnetization. For each sample, loops are presented for the [110] easy axis, [100] hard axis, and the intermediate axis, at $\phi_4=22.5^\circ$.

be well described by the sum of two exponential terms. The demagnetization was calculated for the time delay at which the exponential with the longer relaxation time became dominant. At this point, the electrons and lattice are assumed to have the same temperature and the Kerr signal is assumed to be representative of the spontaneous magnetization. When compared with a hysteresis loop measured with the same 400 nm wavelength probe beam (right hand column) the demagnetization is found to be about 1.4% for A_{300} , 1.0% for A_{400} , and 0.9% for A_{450} . The vertical lines indicate the time delay at which the demagnetization was calculated.

Figure 4(a) shows the results of measurements performed on sample A_{300} , with a magnetic field of 885 Oe applied at different orientations with respect to the crystallographic axes in the field geometry \mathbf{H}_L (refer to Fig. 1). The TRMOKE scans were fitted to Eq. (1) to extract the amplitude, frequency and relaxation rate, with a chirp parameter being used to allow for a change in frequency during the length of the scan. Figures 4(b)–4(e) show the precession amplitude, frequency, relaxation rate and apparent damping parameter, respectively, with error bars obtained from a least-squares minimization fitting procedure.

Measurements made at different field values will be described in the next section. By simultaneously fitting the

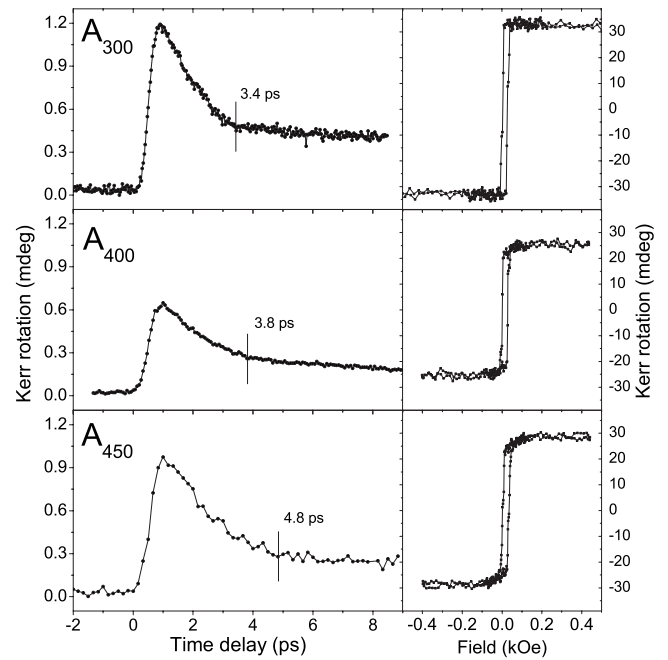


FIG. 3. The transient Kerr rotation signal obtained from samples A_{300} , A_{400} , and A_{450} close to zero time delay with $\phi_4=22.5^\circ$ from the [100] axis in the \mathbf{H}_L configuration. The vertical lines indicate the time delay at which the demagnetization was calculated. The right hand column shows longitudinal MOKE loops measured at $\phi_4=22.5^\circ$ with an s -polarized 400 nm probe beam.

variation of frequency with field strength and orientation using Eq. (4), values of K_1 and g were determined and are presented in Table I. The uncertainty in the value of the magnetization determined in the VSM measurement was approximately 10%. This is the largest contribution to the uncertainties in K_1 and g , which were determined by setting the magnetization to the measured value plus 10% and the measured value minus 10% in the fitting of the precession frequency. The uncertainties in all three parameters are shown in Table I. The perpendicular anisotropy constant $K_{u\perp}$ was set equal to zero during the fitting. The amplitude was fitted by Eq. (3) using the room temperature value of $K_1^{(0)}$ obtained from static MOKE measurements by $K_1^{(0)}=(H_S M_S)/2$, which is equal to -1.3×10^5 erg/cm³ for sample A_{300} . The angular dependence of the relaxation rate was found to be well described by $1/\tau=1/[A \sin(4\phi_4)+B]$, with $A=0.403$ ns and $B=0.815$ ns. The apparent damping parameter in Fig. 5(e) was obtained from the relaxation rate using Eq. (5).

All parameter values in Fig. 4 show a fourfold dependence upon the orientation of the in-plane field. The fourfold variation of the amplitude confirms that precession is induced by an ultrafast modification of the magnetocrystalline anisotropy. When the field is applied parallel to the easy axis ($\phi_4=45, 135^\circ$) or hard axis ($\phi_4=0, 90^\circ$) the amplitude is zero, since no reorientation of the effective field occurs upon a reduction of M_S or K_1 . The precession undergoes a 180° phase change as the static field crosses either of these axes. The data is of sufficient quality that the amplitude in Fig. 4(b) is seen to be a maximum when the static field is applied at 18.5° to the [100] axis rather than at 22.5° as one might

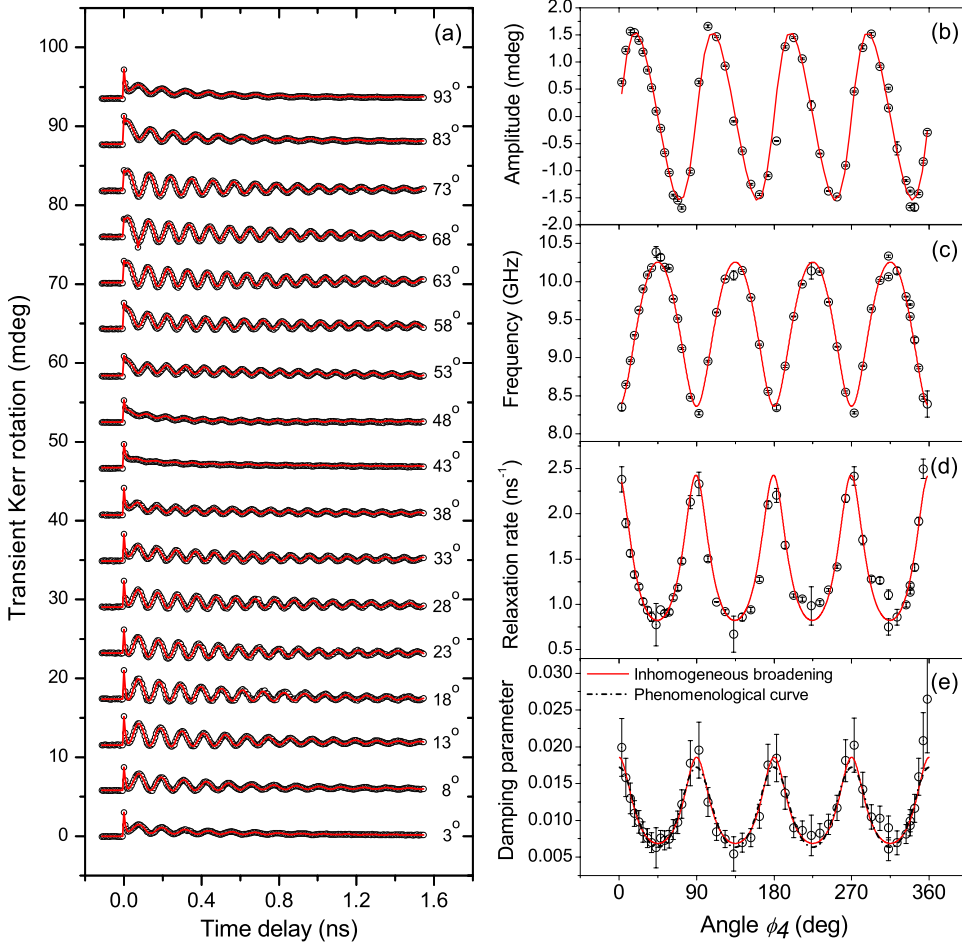


FIG. 4. (Color online) (a) Transient Kerr rotation signals obtained from A_{300} with $H = 885$ Oe and at different ϕ_4 values. The experimental data are fitted to Eq. (1). The variation of (b) the fitted amplitude and (c) the frequency of precession are fitted to Eqs. (3) and (4), respectively, with fitted parameter values given in Table I. The solid line in (d) is a guide to the eye as described in the main text. The red line in (e) is a fit to an inhomogeneous broadening model (10) with fitted parameter values given in Table II, while the dashed black line in (e) is a phenomenological curve calculated from Eq. (11).

initially expect. The canting angle between the magnetization and the external static field is strongly dependent on the magnetocrystalline anisotropy. When the canting angle is calculated as a function of the azimuthal rotation angle ϕ_4 , the maximum value occurs when the static field is oriented at 18.5° from the easy axes.

We observe in Fig. 4(e) that the apparent damping parameter is anisotropic, having a maximum value when the field is parallel to the [100] hard axis (~ 0.018) that is roughly 2.5 times larger than the minimum value that occurs when the field is parallel to the [110] easy axis (~ 0.007). The uncertainty in the calculated damping parameter was obtained by combining the uncertainties in M_S , K_1 , g , and the measured relaxation rate $1/\tau$. The variation of the apparent damping parameter is fitted by the inhomogeneous broadening model [Eqs. (9) and (10)] (red curve), and by a phenomenological curve (dashed black curve) that has the algebraic form,

$$\alpha = C/\{1 - D \cos[4(\phi + \phi_4)]\}, \quad (11)$$

where ϕ is calculated from Eq. (7). The final two terms of Eq. (10) were set equal to zero during the fitting, since their contribution to the total damping was found to be very small. All fitted parameter values are shown in Table II. The uncertainties in the fitted values were obtained by repeating the fitting with the extremal values of M_S , K_1 , and g .

C. Dependence of transient Kerr rotation signals upon the field strength

The dependence of the transient Kerr rotation signal upon magnetic field strength for A_{300} is shown in Fig. 5(a). Again, each TRMOKE scan has been fitted to Eq. (1), with the dependence of the fitted amplitude, frequency, relaxation rate, and apparent damping parameter on the field strength shown in Figs. 5(b)–5(e), respectively. The fitting parameters

TABLE I. The measured and fitted magnetic parameters from static and time-resolved MOKE.

	H_S (Oe)	$M_S (\pm 10\%)$ (emu/cm ³)	g	K_1 (erg/cm ³)	$2K_1/M_S$ (Oe)	$\alpha[110]$	$\alpha[100]$
A_{300}	260	980	1.99 ± 0.09	$-0.84 \pm 0.05 \times 10^5$	-171	0.007 ± 0.002	0.018 ± 0.003
A_{400}	140	1000	1.97 ± 0.09	$-0.46 \pm 0.05 \times 10^5$	-92	0.007 ± 0.003	0.019 ± 0.005
A_{450}	80	1000	1.94 ± 0.09	$-0.26 \pm 0.03 \times 10^5$	-52	0.006 ± 0.003	0.019 ± 0.005

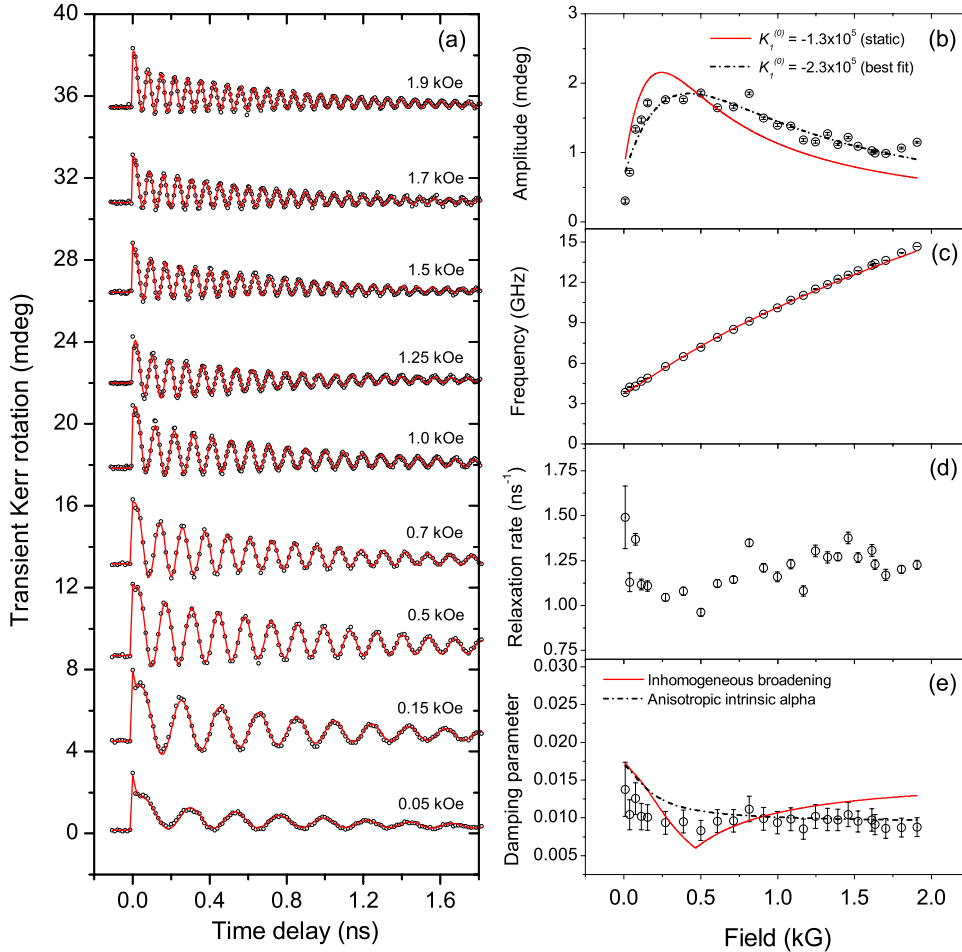


FIG. 5. (Color online) (a) Transient Kerr rotation signals obtained from A_{300} with $\phi_4=22.5^\circ$. The experimental data are fitted to Eq. (1). The field dependence of (b) the fitted amplitude and (c) the fitted precession frequency on the field strength are then fitted to Eqs. (3) and (4), respectively, with fitted parameter values given in Table I. The fitted relaxation rate is shown in (d) while the associated apparent damping parameter is shown in (e). The red curve is a fit to the inhomogeneous broadening model (10) while the black dashed curve in (e) is a phenomenological curve calculated from Eq. (11), with fitted parameter values given in Table II.

are the same as those used to fit the variation of frequency with field orientation in the previous section.

From Fig. 5(b), the measured precession amplitude is seen to gradually decrease as the static magnetic field is increased from 0.5 to 2 kOe. This is consistent with the reduced canting of the magnetization from the external field at higher field values. The amplitude also decreases rapidly when the magnetic field is decreased from 0.2 to 0 kOe, as the magnetization approaches the easy axis. The curve generated from Eq. (3) describes the general trend but has a much sharper maximum. Good agreement is only obtained when the value of $K_1^{(0)}$ is increased to a value much larger than that deduced from the static MOKE magnetometry measurements, as shown in Fig. 5(b). In principle inhomogeneity of K_1 and M_S might lead to broadening of the peak. Numerical calculations showed that while the peak amplitude field value does depend upon K_1 and M_S , reasonable choices of

ΔM_S and ΔK_1 do not produce broadening sufficient to reproduce the experiment. Note also that to fit the frequency in Fig. 5(c) it is essential use the expression for ϕ in Eq. (7).

The apparent damping parameter α appears to be independent of the applied field strength until the field is reduced to less than 0.2 kOe. For fields greater than 0.2 kOe, the value of $\alpha=0.009$ is consistent with that found in the azimuthal scan shown in Fig. 4(f) at $\phi_4=22.5^\circ$. Again the apparent damping parameter is fitted to the inhomogeneous broadening model (red curve) while the black dashed curve is obtained from Eqs. (11) and (7). The inhomogeneous broadening model does not describe the field dependence of the apparent damping parameter particularly well, producing a sharply peaked minimum that is not seen in the experimental data, and predicting an increase at larger field values while the data shows an approximately constant value.

TABLE II. Fitted parameter values from the inhomogeneous broadening model and phenomenological curve

	α_{constant}	ΔM_S (emu/cm ³)	ΔK_1 (erg/cm ³)	$\Delta K_1/K_1$	C	D
A_{300}	0.006	50 ± 6	$0.17 \pm 0.03 \times 10^5$	20%	0.009	0.46
A_{400}	0.006	71 ± 9	$0.13 \pm 0.04 \times 10^5$	28%	0.009	0.47
A_{450}	0.005	72 ± 9	$0.16 \pm 0.04 \times 10^5$	62%	0.010	0.50

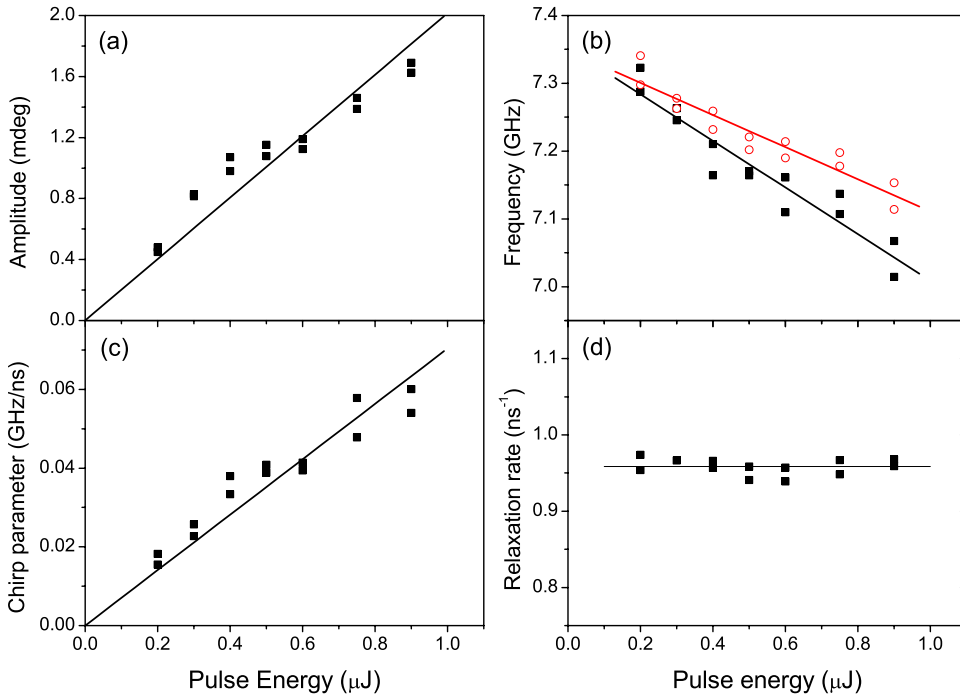


FIG. 6. (Color online) The dependence of (a) amplitude, (b) frequency, (c) chirp parameter, and (d) relaxation rate upon the energy of the pump pulse are shown for measurements made on sample A_{300} with a field of 445 Oe applied parallel to the plane of incidence and at $\phi_4 = 22.5^\circ$. In (b), the circles were determined from fits to Eq. (1), while the squares were obtained from fast Fourier transforms. In all panels, the solid lines are guides to the eye.

D. Dependence of transient Kerr rotation signals upon the pump pulse energy and spot size

Measurements were performed for a range of pump pulse energies in order to detect the presence of damping mechanisms that depend upon the amplitude of precession. The average power of the pump beam was measured with a standard power meter to an accuracy of about 10%. Figure 6 shows the variation of (a) amplitude, (b) frequency, (c) chirp parameter, and (d) relaxation rate with pump pulse energy for sample A_{300} . The amplitude increases linearly with pulse energy up to $0.9 \mu\text{J}$, while the frequency decreases linearly. Two sets of data are presented for the frequency: values obtained from the fit to Eq. (1) and values obtained from fast Fourier transform (FFTs) of the TRMOKE scans. The FFT gives an average frequency over the entire scan period (2–3 ns), while the fit, when a chirp parameter is used, gives the frequency at the beginning of each scan. For the maximum pulse energy used, the frequency obtained from the FFT is smaller by about 3%, while that determined by the fitting is smaller by about 4%, relative to the extrapolated value at zero pump energy. This can be understood as a thermal effect whereby the magnetic parameters (magnetization and magnetocrystalline anisotropy) of the sample undergo a larger ultrafast modification at zero time delay when a higher pump pulse energy is used. The frequency also changes more rapidly in time, giving rise to an increased chirp parameter [Fig. 6(c)]. For the maximum pulse energy used, the chirp parameter of 0.06 GHz/ns implies an increase in frequency of 0.18 GHz, or about 2%, during a 3 ns scan. The relaxation rate [Fig. 6(d)], and hence the apparent damping parameter, are not affected by the pump pulse energy within the range of values used in the present experiments.

A possible origin of inhomogeneity in all-optical TRMOKE is the spatially nonuniform intensity profile of the pump laser spot. The nonuniform pumping mechanism could

lead to generation of spin waves that carry energy away from the probed region. If this is a significant factor then changing the size of the pump spot relative to the probe should result in a different value of the relaxation rate. In fact, we found that doubling the pump spot diameter with a constant probe spot size made little difference to the observed relaxation rates. Therefore, we can say that the nonuniform pump intensity has a negligible contribution to the total apparent damping in this case.

E. Dependence of the precession frequency upon the annealing temperature

Time-resolved measurements were also made on samples annealed at 400°C (A_{400}) and 450°C (A_{450}). Annealing at higher temperatures is known to improve the site ordering of these films, and changes in the structure and electronic state are expected to influence the magnetic properties.³⁸ The static MOKE loops in Fig. 2 show a reduction in the magnetocrystalline anisotropy, K_1 , with increasing annealing temperature. The smaller magnetocrystalline anisotropy in turn leads to a smaller amplitude precession in TRMOKE measurements. While smaller static field values were used to increase the precession amplitude, the values of 440 Oe for A_{400} and 475 Oe for A_{450} are still sufficient to produce a uniformly magnetized state.

Due to the reduced magnetocrystalline anisotropy the amplitude of precession and hence the signal to noise ratio of the TRMOKE data is worse for A_{400} and A_{450} compared to A_{300} . For sample A_{450} , TRMOKE signals were recorded in the transverse field geometry (\mathbf{H}_T in Fig. 1) as the field strength was varied. This yielded somewhat larger oscillatory Kerr signals, and explains why larger signals are seen for A_{450} relative to A_{400} .

Transient Kerr rotation signals were again fitted to Eq. (1), but with the chirp parameter set to zero due to the some-

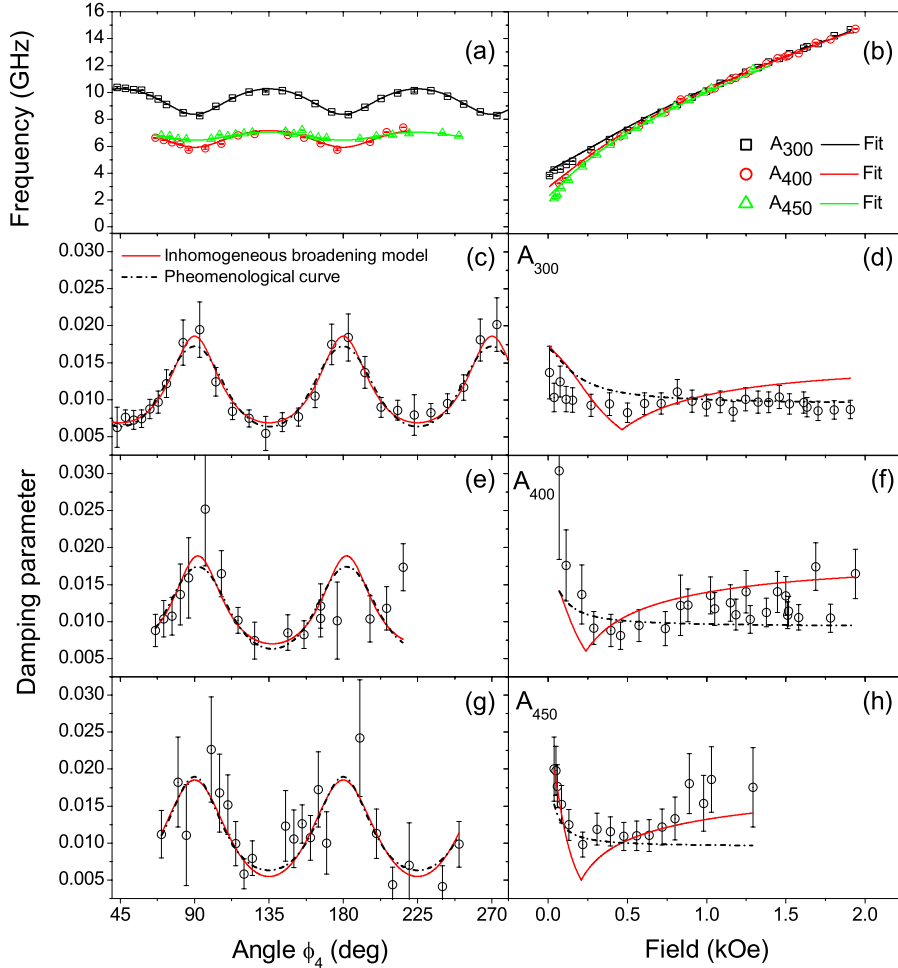


FIG. 7. (Color online) The results of TRMOKE measurements on samples A_{300} , A_{400} , and A_{450} . (a) and (b) show the dependence of the precession frequency on field orientation and strength, respectively. The remaining panels show the variation of the apparent damping parameter with field strength and orientation for all three samples. The red curves are the fit to the inhomogeneous broadening model, while the black dashed curves correspond to a phenomenological expression fitted to the data.

what lower quality of the raw data. Figures 7(a) and 7(b) show the variation of precession frequency with field orientation and field strength, respectively, for all three annealing temperatures. Although the variation of the precession frequency in Fig. 7(a) is much smaller for A_{400} and A_{450} compared to that observed for A_{300} , the fourfold symmetry is still clear. The frequency versus field strength scans are nearly identical at high field for all three samples [Fig. 7(b)], indicating that M_S is very similar for all three samples. The dependence of the apparent damping parameter on the field orientation is shown in Figs. 7(c), 7(e), and 7(g), and variation with field strength in Figs. 7(d), 7(f), and 7(h), for samples A_{300} , A_{400} , and A_{450} , respectively. The apparent damping parameter values in Figs. 7(e) and 7(g) show strong scatter near the easy and hard axis orientations due to the small amplitude of the Kerr rotation. The fitted magnetic parameters and extracted damping parameters are presented in Table I, along with the values of the saturation magnetization determined by VSM and hard axis saturation field H_S from the static MOKE measurements.

The dependence of the apparent damping parameter upon H for $H > 0.5$ kOe is quite different for A_{400} and A_{450} when compared to A_{300} . For A_{300} , the apparent damping parameter appears to be constant above 500 Oe, while for A_{400} and A_{450} it increases with field. The anisotropy of the apparent damping parameter is rather similar for all three annealing temperatures. For all three samples, the variation of the apparent

damping with field orientation can be well fitted by the inhomogeneous broadening model with a constant offset, while the same model reproduces the trends in the field dependent data for all but A_{300} . The parameter values obtained from fitting to the inhomogeneous broadening model are shown in Table II. Due to their relatively weak influence on the total damping, the dispersion in the perpendicular anisotropy ($\Delta K_{u\perp}$) and the magnetization orientation ($\Delta\phi_4$) were set equal to zero. The dispersion in the anisotropy constant, ΔK_1 , is found to be similar for all three samples at around 0.15×10^5 erg/cm³, even though this represents a larger percentage variation for A_{450} . The phenomenological expression (black dashed curve in figures) yields a reasonable description of the angular variation of α for all three samples, however for samples A_{400} and A_{450} the increase in the apparent damping parameter at higher fields is only reproduced by the inhomogeneous broadening model.

V. DISCUSSION

The static magnetic properties of the samples in the present study are seen to be distinctly different to those reported previously for nominally similar samples.⁶ VSM measurements have shown that the value of the spontaneous magnetization M_S is close to that of the bulk material in all three samples in this study and so appears to be unaffected by the annealing treatment. This finding is supported by the

dependence of the precession frequency upon field strength shown in Fig. 7(b). The curves for the three samples are almost exactly overlaid at high field values, suggesting that the effective demagnetizing field is very similar in each case. The film thickness of 30 nm is rather too large for surface anisotropy fields to be significant, while there is no suggestion from x-ray measurements of a tetragonal distortion in the direction normal to the film. While the values of K_1 deduced from the MOKE hysteresis loops of Fig. 2 are larger than those reported by Gaier *et al.*,⁶ we observe a similarly dramatic decrease of K_1 with increasing annealing temperature. Gaier *et al.* suggested that diffusion of Cr from the buffer layer may lead to a reduction in the magnetization as the annealing temperature is increased. In the present study, no significant reduction in the magnetization is observed for annealing temperatures in the range of 300–450 °C, suggesting that Cr diffusion is not a significant factor.

The variation of the precession amplitude with the orientation of the applied magnetic field shown in Fig. 4 confirms that magnetization precession is induced by ultrafast optical modification of the magnetocrystalline anisotropy field. From an analysis of the measured magnetization dynamics,³⁹ Jozsa *et al.* have shown that optical modification of the magnetic anisotropy can generate a transient effective magnetic field. This magnetic field consisted of an initial pulse of <5 ps duration, and a steplike longer lived component, the latter being more effective in stimulating precessional dynamics. Consequently, only a steplike perturbation has been included within our model. The experimental data of Figs. 4 and 5 is well described by the simple model presented previously, with the exception of the dependence of the Kerr amplitude upon field strength shown in Fig. 5(b). This is most likely due to the occurrence of spatial nonuniformity of the magnetization, which is not taken into account within the model, when the applied field is smaller than the anisotropy field. The values of $2K_1/M_S$ deduced from pump-probe experiments shown in Table I are significantly smaller than those deduced from MOKE magnetometry at room temperature. This may be attributed to the local increase in temperature induced by the pump pulse during the time-resolved MOKE measurements. The pump-induced demagnetization was deduced from Fig. 3 for time delays at which nonthermal modification of the optical constants can be neglected and at which the electron and phonon systems can be assumed to have reached a common temperature. While the optically induced demagnetization was found to be about 1% for all three samples, the reduction of $2K_1/M_S$ deduced from the dependence of the precession frequency upon field orientation in Fig. 7(a) was about 35% for all three samples. The reduction of K_1 deduced for A_{300} is also consistent with the dependence of the precession frequency upon pump pulse energy shown in Fig. 6(b). The variation of the precession frequency is dominated by the variation of the $2K_1/M_S$ term within the expression for H_β in Eq. (4). The 3% reduction in the precession frequency at short delay times for pulse energy of 0.6 μJ requires $2K_1/M_S$ to be reduced by 35%. For bulk materials, theory predicts³⁶ that $K_1(T) \sim M(T)^n$, with $n=10$, so that the pump-induced demagnetization should lead to a fractional change in $2K_1/M_S$ given by,

$$\Delta \left(\frac{K_1(T)}{M(T)} \right) / \left(\frac{K_1(T)}{M(T)} \right) = (n-1) \frac{\Delta M(T)}{M(T)}. \quad (12)$$

A demagnetization of about 1% should then lead to a change in $2K_1/M_S$ of about 10% that is significantly smaller than the observed values. This suggests the presence of other pump-induced contributions to the anisotropy energy, such as magneto-elastic anisotropy associated with thermal expansion⁴⁰ and magnetoelastic coupling,⁴¹ which has been inferred previously when larger values of n have been observed.³⁵

While the dependence of the frequency of precession upon field strength and orientation is generally well described by the model using constant values of M_S , g , and K_1 for a particular sample, Fig. 7 shows that the apparent damping parameter α must vary significantly for the model to reproduce the observed variation of the relaxation rates with field strength and orientation. It is first necessary to consider whether the variation of α is either an artifact associated with the TRMOKE measurement technique or specific to the experimental conditions employed. Figure 6 shows that while the amplitude of precession increases monotonically, the relaxation rate and hence α are constant as the pump fluence is increased. This suggests that nonlinear effects such as three and four magnon scattering do not contribute to the observed damping. The intensity of the focused pump beam may be assumed to have a Gaussian radial dependence, which implies that the initial temperature change and hence the frequency of precession also depend upon the distance from the center of the pump spot. By weighting the signals obtained from annuli of different radius by the probe intensity, which is itself described by a Gaussian function of smaller width, a frequency distribution function may be obtained. The full width at half maximum (FWHM) of this curve may then be inserted into Eq. (9), from which it is found that dephasing of signals associated with different distances from the spot center should contribute less than 15% of the total observed relaxation rate. The radial variation of the amplitude of precession could also lead to the propagation of long wavelength magnetostatic spin waves out of the probed region, leading again to an increase in the observed relaxation rate.²⁵ The effect is anisotropic with surface modes propagating perpendicular to the magnetization with a group velocity that is an order of magnitude greater than that of the backward volume waves that propagate parallel to the magnetization. A rough estimate suggests that the surface waves may propagate a distance up to about 30 μm within the 3 ns range of time delay used in the experiments. This effect may therefore have some small influence upon the relaxation rate determined with a probe spot of 80 μm diameter. However, the most direct evidence that inhomogeneous excitation does not significantly contribute to the observed relaxation comes from the observation that the relaxation rate was unaffected when the diameter of the pump spot was doubled.

The phenomenological expression in Eq. (11) is seen to give a good description of the dependence of α upon field orientation, but a poor account of the dependence of α upon field strength within Fig. 7. The inhomogeneous broadening model, Eq. (10), is able to reproduce the dependence of α

upon field orientation and the increase in α seen at large fields for A_{400} and A_{450} . However, it overestimates the variation of α at high fields for A_{300} . While the model shows an upturn in α at low field, it is again questionable whether the model is applicable in this regime, since the static magnetization may become spatially nonuniform, and so the lack of quantitative agreement is unsurprising. From Table II, it is seen that the fit to the model is able to describe the data for all three samples with a constant contribution to α of 0.006 for samples A_{300} and A_{400} , and 0.005 for sample A_{450} . The fractional dispersion in M_S is about 5% to 7% for all three samples while the fractional dispersion in K_1 is much larger. This seems reasonable since K_1 appears to differ greatly for the B2 and L2₁ phases, so there should be strong dispersion of K_1 for a film containing both phases. The absolute dispersion of K_1 is of similar magnitude for all three samples, while the fractional dispersion of K_1 increases with increased annealing temperature. An alternative explanation of the variation of the value of α may be provided by two-magnon scattering from a fourfold network of misfit dislocations, as reported previously for epitaxial thin films.^{17,18} However, further structural studies are required to confirm the presence of such dislocations in the present case, and further theoretical work is required to demonstrate that this mechanism yields the correct dependence of α upon the strength and orientation of the applied field. In those studies, the Fe films were subjected to a lattice strain by a mismatch with an underlying Pd layer, giving rise to dislocations with the same rotational symmetry as the Fe films. While in this case, the Co₂MnSi films are well lattice-matched to the substrate, growth by sputter deposition could introduce a similar network of defects that are not fully removed by the annealing process.

Comparing the values of α in Fig. 7 and Table II with those reported by Yilgin *et al.*, there are a number of significant differences. The values obtained from TRMOKE are larger than those from FMR, and in the TRMOKE measurements the inhomogeneous broadening model can largely account for the variation of the apparent damping parameter without the need for an anisotropic intrinsic damping. The samples studied by Yilgin *et al.* were slightly Co rich (Co:Mn:Si=54.6:23.5:21.9), and it is known that the composition can affect the annealing temperature dependence of the damping parameter. It is possible that the TRMOKE and FMR techniques yield different values due to the different volumes of material sampled. However, TRMOKE samples a small spot of 100 μm size while in FMR, the entire 10 mm² sample is placed within the microwave cavity, so inhomogeneous broadening is expected to be more severe in the case of FMR.²³ The smaller values of α obtained by Yilgin *et al.* may in part be due to the different methods used to account for the contribution of inhomogeneous broadening to the FMR linewidth. Also, it should be noted that the beam from the regenerative laser amplifier system may become very slightly divergent or convergent as the alignment of the amplifier is adjusted from day to day. The focusing of the pump and probe spots is performed with the optical delay line set for short time delays. However, if the pump beam passing through the delay line is not exactly parallel, then the size of the focused spot may increase when the path length is

changed so that the amplitude of the oscillatory Kerr signal is reduced giving the impression of a somewhat larger damping. The diameter of the pump spot would need to increase by approximately 50% over the duration of the measurement to explain the difference in the values of α deduced from the TRMOKE and FMR studies.

The present study has therefore shown that the site ordering that results from annealing Co₂MnSi films can lead to a dramatic change in the value of K_1 while the values of M_S , g and the constant contribution to α are not greatly affected, even though the values of K_1 and α both originate from the spin-orbit interaction. While the slight variation of the fitted g factor in Table I with annealing temperature is probably not significant, the fact that the value is just less than 2 for all three samples suggests that in each case the orbital moment is small and antiparallel to the spin moment. The small orbital moment also accounts for the relatively small values of α since the values of α and $g-2$ are generally found to be correlated.⁴² However, the magnetocrystalline anisotropy depends instead upon the anisotropy of the orbital moment as it is aligned parallel to different crystallographic axes. Annealing presumably enhances the strength of the crystal field and leads to a reduction in both the size and anisotropy of the orbital moment, and hence to the observed reduction in the magnetocrystalline anisotropy.

VI. SUMMARY

In summary, all-optical pump-probe measurements of precessional magnetization dynamics have been presented for epitaxial Co₂MnSi thin films in which precession of the magnetization is induced by an ultrafast reduction in the magnetocrystalline anisotropy field. A simple model allows the values of the effective fields within the sample to be deduced from the dependence of the frequency of precession upon the strength and orientation of the applied magnetic field. While the magnetocrystalline anisotropy constant is greatly reduced with increased annealing temperature, the magnetization remains almost unchanged, and therefore it is unlikely that the reduction in anisotropy is the result of diffusion from the Cr buffer layer. The model also allows an apparent damping parameter α to be determined from the observed relaxation of the oscillatory Kerr rotation signal. This apparent damping parameter exhibits a strong dependence upon the strength and orientation of the applied field. The dependence of α upon the field orientation is well described by an inhomogeneous broadening model in which there is a constant contribution to the observed damping that includes an intrinsic contribution and strong dispersion in the value of the cubic magnetocrystalline anisotropy constant, K_1 . The inhomogeneous broadening model provides a good description of the field dependence of the apparent damping parameter for samples annealed at temperatures of 400 and 450 °C, but not for that annealed at 300 °C. This may imply that two-magnon scattering from a fourfold network of misfit dislocations contributes to the observed damping behavior. The strong dispersion of K_1 , invoked within the inhomogeneous broadening model for samples of mixed phase, is a consequence of the large difference in the values of K_1 for the B2

and $L2_1$ phases. Annealing leads to an increased fraction of the $L2_1$ phase and a reduction in the measured K_1 value, while the constant contribution to α remains unchanged. These conclusions may be understood if the orbital moments are small for both phases, but the anisotropy of the orbital moment is reduced in the $L2_1$ phase relative to the B2 phase. Finally, this work demonstrates the potential of the optical pump-probe measurement technique for the study of dynamical magnetic properties in microscopic samples where the

addition of planar waveguides for the delivery of pulsed magnetic fields is either undesirable or infeasible.

ACKNOWLEDGMENTS

The authors gratefully acknowledge the financial support of the Engineering and Physical Sciences Research Council (EPSRC) and the New Energy and Development Organization (NEDO).

- ¹I. Galanakis, P. H. Dederichs, and N. Papanikolaou, *Phys. Rev. B* **66**, 174429 (2002).
- ²Y. Sakuraba, J. Nakata, M. Oogane, H. K. Y. Ando, A. Sakuma, and T. Miyazaki, *Jpn. J. Appl. Phys.* **44**, L1100 (2005).
- ³Y. Sakuraba, M. Hattori, M. Oogane, Y. Ando, H. Kato, A. Sakuma, T. Miyazaki, and H. Kubota, *Appl. Phys. Lett.* **88**, 192508 (2006).
- ⁴G. de Loubens, A. Riegler, B. Pigeau, F. Lochner, F. Boust, K. Y. Guslienko, H. Hurdequint, L. W. Molenkamp, G. Schmidt, A. N. Slavin, V. S. Tiberkevich, N. Vukadinovic, and O. Klein, *Phys. Rev. Lett.* **102**, 177602 (2009).
- ⁵M. Oogane, Y. Sakuraba, J. Nakata, H. Kubota, Y. Ando, A. Sakuma, and T. Miyazaki, *J. Phys. D* **39**, 834 (2006).
- ⁶O. Gaier, J. Hamrle, S. J. Hermsdoerfer, H. Schultheiß, B. Hillebrands, Y. Sakuraba, M. Oogane, and Y. Ando, *J. Appl. Phys.* **103**, 103910 (2008).
- ⁷P. J. Brown, K. U. Neumann, P. J. Webster, and K. R. A. Ziebeck, *J. Phys.: Condens. Matter* **12**, 1827 (2000).
- ⁸L. Chioncel, Y. Sakuraba, E. Arrigoni, M. I. Katsnelson, M. Oogane, Y. Ando, T. Miyazaki, E. Burzo, and A. I. Lichtenstein, *Phys. Rev. Lett.* **100**, 086402 (2008).
- ⁹N. D. Telling, P. S. Keatley, G. van der Laan, R. J. Hicken, E. Arenholz, Y. Sakuraba, M. Oogane, Y. Ando, and T. Miyazaki, *Phys. Rev. B* **74**, 224439 (2006).
- ¹⁰N. D. Telling, P. S. Keatley, L. R. Shelford, E. Arenholz, B. van der Laan, R. J. Hicken, Y. Sakuraba, S. Tsunegi, M. Oogane, Y. Ando, K. Takanashi, and T. Miyazaki, *Appl. Phys. Lett.* **92**, 192503 (2008).
- ¹¹L. R. Shelford, Y. Liu, R. J. Hicken, Y. Sakuraba, M. Oogane, and Y. Ando, *J. Appl. Phys.* **103**, 07D720 (2008).
- ¹²R. Yilgin, Y. Sakuraba, M. Oogane, S. Mizukami, Y. Ando, and T. Miyazaki, *Jpn. J. Appl. Phys.* **46**, L205 (2007).
- ¹³W. Platow, A. N. Anisimov, G. L. Dunifer, M. Farle, and K. Baberschke, *Phys. Rev. B* **58**, 5611 (1998).
- ¹⁴S. Mizukami, Y. Ando, and T. Miyazaki, *Phys. Rev. B* **66**, 104413 (2002).
- ¹⁵G. Malinowski, K. C. Kuiper, R. Lavrijsen, H. J. M. Swagten, and B. Koopmans, *Appl. Phys. Lett.* **94**, 102501 (2009).
- ¹⁶J. F. Cochran, R. W. Qiao, and B. Heinrich, *Phys. Rev. B* **39**, 4399 (1989).
- ¹⁷B. Heinrich, G. Woltersdorf, R. Urban, O. Mosendz, G. Schmidt, P. Bach, L. Molenkamp, and E. Rozenberg, *J. Appl. Phys.* **95**, 7462 (2004).
- ¹⁸G. Woltersdorf, B. Heinrich, J. Woltersdorf, and R. Scholz, *J. Appl. Phys.* **95**, 7007 (2004).
- ¹⁹A. A. Rzhevsky, B. B. Krichevtsov, D. E. Bürgler, and C. M. Schneider, *J. Appl. Phys.* **104**, 083918 (2008).
- ²⁰M. Djordjevic, G. Eilers, A. Parge, M. Münzenberg, and J. S. Moodera, *J. Appl. Phys.* **99**, 08F308 (2006).
- ²¹G. Woltersdorf, M. Buess, B. Heinrich, and C. H. Back, *Phys. Rev. Lett.* **95**, 037401 (2005).
- ²²G. M. Müller, M. Münzenberg, G. X. Miao, and A. Gupta, *Phys. Rev. B* **77**, 020412(R) (2008).
- ²³I. Neudecker, G. Woltersdorf, B. Heinrich, T. Okuno, G. Gubbiotti, and C. H. Back, *J. Magn. Magn. Mater.* **307**, 148 (2006).
- ²⁴G. Eilers, M. Lüttich, and M. Münzenberg, *Phys. Rev. B* **74**, 054411 (2006).
- ²⁵J. Wu, N. D. Hughes, J. R. Moore, and R. J. Hicken, *J. Magn. Magn. Mater.* **241**, 96 (2002).
- ²⁶Q. Zhang, A. V. Nurmikko, A. Anguelouch, G. Xiao, and A. Gupta, *Phys. Rev. Lett.* **89**, 177402 (2002).
- ²⁷H. B. Zhao, D. Talbayev, Q. G. Yang, G. Lüpke, A. T. Hanbicki, C. H. Li, O. M. J. van't Erve, G. Kioseoglou, and B. T. Jonker, *Appl. Phys. Lett.* **86**, 152512 (2005).
- ²⁸D. Talbayev, H. Zhao, G. Lüpke, A. Venimadhav, and Q. Li, *Phys. Rev. B* **73**, 014417 (2006).
- ²⁹Y. Liu, L. R. Shelford, V. V. Kruglyak, R. J. Hicken, Y. Sakuraba, M. Oogane, Y. Ando, and T. Miyazaki, *J. Appl. Phys.* **101**, 09C106 (2007).
- ³⁰A. A. Rzhevsky, B. B. Krichevtsov, D. E. Bürgler, and C. M. Schneider, *Phys. Rev. B* **75**, 224434 (2007).
- ³¹H. Kubota, J. Nakata, M. Oogane, Y. Ando, H. Kato, A. Sakuma, and T. Miyazaki, *J. Appl. Phys.* **97**, 10C913 (2005).
- ³²J. A. C. Bland, M. J. Padgett, R. J. Butcher, and N. Bett, *J. Phys. E* **22**, 308 (1989).
- ³³C. Daboo, J. A. C. Bland, R. J. Hicken, A. J. R. Ives, M. J. Baird, and M. J. Walker, *Phys. Rev. B* **47**, 11852 (1993).
- ³⁴E. Beaurepaire, J. C. Merle, A. Daunois, and J. Y. Bigot, *Phys. Rev. Lett.* **76**, 4250 (1996).
- ³⁵C. Zener, *Phys. Rev.* **96**, 1335 (1954).
- ³⁶A. H. Morrish, *The Physical Principles of Magnetism* (Wiley, New York, 1965), Chap. 6.
- ³⁷J. Hamrle, S. Blomeier, O. Gaier, B. Hillebrands, H. Schneider, G. Jakob, K. Postava, and C. Felser, *J. Phys. D* **40**, 1563 (2007).
- ³⁸R. Yilgin, M. Oogane, S. Yakata, Y. Ando, and T. Miyazaki, *IEEE Trans. Magn.* **41**, 2799 (2005).
- ³⁹C. Jozsa, J. H. H. Rietjens, M. van Kampen, E. Smalbrugge, M. K. Smit, W. J. M. de Jonge, and B. Koopmans, *J. Appl. Phys.* **95**, 7447 (2004).
- ⁴⁰W. J. Carr, *J. Appl. Phys.* **31**, 69 (1960).
- ⁴¹E. R. Callen and H. B. Callen, *Phys. Rev.* **129**, 578 (1963).
- ⁴²J. Pelzl, R. Meckenstock, D. Spoddig, F. Schreiber, J. Pflaum, and Z. Frait, *J. Phys.: Condens. Matter* **15**, S451 (2003).